Nuclear Materials and Energy 18 (2019) 159–165

Contents lists available at ScienceDirect

Nuclear Materials and Energy

journal homepage: www.elsevier.com/locate/nme

Stationarity of I-mode operation and I-mode divertor heat fluxes on the ASDEX Upgrade tokamak

T. Happel[*,a], M. Griener[a,b], D. Silvagni[a,b], S.J. Freethy[a,c], P. Hennequin[d], F. Janky[a], P. Manz[a,b], D. Prisiazhniuk[a,b], F. Ryter[a], M. Bernert[a], D. Brida[a], T. Eich[a], M. Faitsch[a], L. Gil[e], L. Guimarais[e], A. Merle[f], D. Nille[a], J. Pinzón[a,b], B. Sieglin[a], U. Stroth[a,b], E. Viezzer[g], the ASDEX Upgrade Team[1], the EUROfusion MST1 Team[2]

[a] Max-Planck-Institut für Plasmaphysik, Boltzmannstr. 2, Garching, 85748 Germany
[b] Physik-Department E28, Technische Universität München, James-Franck-Str. 1, Garching, 85748 Germany
[c] Plasma Science and Fusion Center, Massachusetts Institute of Technology, Cambridge, Massachusetts 02139, USA
[d] Laboratoire de Physique des Plasmas, Ecole Polytechnique, Palaiseau, 91128 France
[e] Instituto de Plasmas e Fusão Nuclear, Instituto Superior Técnico, Universidade de Lisboa, Portugal
[f] Ecole Polytechnique Fédérale de Lausanne (EPFL), Swiss Plasma Center (SPC), Lausanne, CH-1015 Switzerland
[g] Dept. of Atomic, Molecular and Nuclear Physics, University of Seville, Seville, Spain

A B S T R A C T

Recent I-mode investigations from the ASDEX Upgrade tokamak are reported. It is shown that neutral-beam-injection heated I-modes can be stationary, which is important in terms of extrapolability towards future fusion devices. Furthermore, detailed studies on the weakly coherent mode are reported. In particular, experimental observations point towards its existence in L-mode, before I-mode starts. Moreover, its impact on density and temperature fluctuations is evaluated. Studies of stationary divertor heat fluxes show that in I-mode, the upstream power fall-off length is between those observed in L-mode and H-mode, and it is connected to the scrape-off layer temperature fall-off length. Moreover, analysis of transient divertor heat loads shows that intermittent turbulent events, observed in the confinement region and linked to the weakly coherent mode, are responsible for a significant part of divertor heat loads.

1. Introduction

The I-mode is an improved energy confinement regime of tokamak plasmas which can be accessed when the H-mode power threshold is kept high. This can be achieved by using magnetic configurations with the ion grad B drift pointing away from the active X-point, i.e. the so-called unfavorable configurations in terms of H-mode access. I-modes are characterized by L-mode like particle transport while heat transport is reduced in the edge plasma [1,2]. As a consequence, a temperature pedestal is formed, while no pedestal is observed in the density. Impurity transport properties in I-mode are benevolent, and impurity accumulation has so far not been observed [3], which has recently been proposed to be due to neoclassical impurity removal [4]. The I-mode is usually accompanied by an edge instability called the weakly coherent mode (WCM), which has been investigated intensively in the last few years [5–8]. It has been suggested that the WCM might be responsible for the comparably strong particle transport in I-mode [5,8], and in fact, the WCM is related to intermittent turbulent events which are generated in the edge plasma, but inside the confinement region [9]. These turbulent "bursts" expel particles and energy from the confined plasma which end up in the divertor [10]. Since the I-mode is a natural ELM-free regime [10,11], it might be suitable for a future fusion reactor [12]. In particular, some future high magnetic field devices are planning to explore I-mode in detail [13,14]. In I-mode, the scrape-off layer temperature fall-off length λ_T is short [15], which usually leads to a short upstream power fall-off length λ_q [16,17]. However, it has been shown that λ_q in I-mode can be comparably large, at least larger than in H-mode [18].More recent studies from Alcator C-Mod show that $\lambda_q$scales inversely with the volume-averaged plasma pressure, obtaining a unified scaling law which holds over all confinement regimes explored (L-mode, I-mode, H-mode) [19].

This paper reports on recent I-mode investigations on the ASDEX Upgrade tokamak (AUG). First, it is shown that stationary I-modes can be obtained with neutral-beam-injection heating, which has been achieved in 2017 for the first time. Furthermore, measurements are reported which indicate that the WCM is not I-mode exclusive on AUG.

* Corresponding author.
E-mail address: tim.happel@ipp.mpg.de (T. Happel).
[1] see the author list "A. Kallenbach et al., *Nucl. Fusion* **57**, *102015 (2017)*"
[2] see the author list "H. Meyer et al., *Nucl. Fusion* **57**, *102014 (2017)*"

https://doi.org/10.1016/j.nme.2018.12.022
Received 30 July 2018; Received in revised form 5 December 2018; Accepted 19 December 2018
Available online 26 December 2018

Nevertheless, it is likely that the WCM plays an important role in I-mode transport because of its dominance in the turbulence spectrum: in L-mode, the WCM is barely visible in the density fluctuation spectrum, while in I-mode, most of the turbulence away from the WCM frequencies is reduced. First investigations of divertor heat fluxes and the SOL power fall-off length in I-mode have been reported for Alcator C-Mod [18,19]. The present paper contributes measurements from AUG, and shows that indeed, I-mode values for λ_q are larger than those for H-mode, but also smaller than in L-mode. Moreover, transient divertor heat loads are investigated, and it is shown that the intermittent turbulent events, which are observed in the confinement region and linked to the WCM, contribute substantially to the divertor heat fluxes.

This paper is organized as follows: Section 2 introduces newly obtained stationary I-modes obtained with NBI heating. Section 3 investigates the WCM in detail, showing its existence in both density and temperature, and that it is not exclusive to I-mode. This is followed by a more detailed discussion of both stationary and transient divertor heat loads during I-mode in Section 4. Section 5 summarizes the results of this paper.

2. Stationarity with neutral beam injection

On AUG, before 2017, stationary I-modes could only be obtained with electron cyclotron resonance heating (ECRH). If neutral beam injection (NBI) was applied, even at fixed power, the plasma edge profiles would evolve on timescales longer than the energy confinement time, and eventually a transition from I-mode to H-mode would occur [20]. This is attributed to the fact that the existence window for I-mode is comparably narrow on AUG, which normally operates at a magnetic field strength of 2.5 T. Alcator C-Mod has shown that the I-mode existence window opens up at higher magnetic field strengths [21]. In fact, no I-H transitions were observed in recent studies at 8 T on Alcator C-Mod [12].

To obtain stationary I-modes, NBI power feedback control has recently been applied to AUG I-mode discharges. The feedback was programmed to react on the value of the poloidal plasma beta, β_{pol}. Fig. 1 shows an AUG discharge in which the (modulated) NBI power is ramped linearly in the very beginning of the time window (panel (a)). At $t = 2.48$ s, the L-I transition takes place, which can be observed in the pedestal top ion and electron temperatures (panel (b)), which go from $T_{ped} = 0.30$ to 0.45 keV in I-mode at $t = 2.7$ s. The improved confinement is also visible in the plasma stored energy W (panel (c)), which shows a kink at $t = 2.48$ s. Fig. 1(d) shows the preprogrammed β_{pol} request value (black), and the β_{pol} time trace which was actually achieved(magenta). Feedback is switched on at $t = 2.516$ s (magenta line starts). Since I-mode has already been entered at this point, β_{pol} is rising and above the request value. Therefore, the NBI power is reduced (panel (a)), and irrespective of this input power reduction, T_{ped} and W continue to rise. This reduction of NBI input power is crucial to obtain stationary I-modes on AUG. During the L-I transition, the density (panel (e)) stays roughly constant.

In the subsequent I-mode phase, the request of the β_{pol} value is stepped three times, at $t = 3.1$, 3.8 and 4.5 s. Both T_{ped} and W follow these steps due to an increase in NBI power, while the density is unaffected, which is typical for I-mode. In panels (g) and (h), the electron temperature and density profiles obtained via the integrated data analysis (IDA) framework [22] are shown, respectively, for three different time windows indicated with vertical bars in Fig. 1(e). The electron temperature continuously increases in I-mode with respect to the L-mode profile, while the density profile is unchanged. Note that the confinement improvement factor $H_{98}(y, 2)$ [23] is indicated in (g). It is 0.65 for the L-mode time window, while in I-mode it is 0.81 and 0.89. On AUG, stationary I-modes are usually observed at $H_{98}(y, 2) < 0.85$, while at Alcator C-Mod, values of up to 1.3 have been observed [21]. The question remains whether this difference could be due to the higher magnetic field strength of C-Mod, which tends to widen the I-mode existence window in terms of input power. Since power degradation in I-mode is small ($\tau_E \propto P^{-0.28}$) [2,11,21] compared to H-mode ($\tau_E \propto P^{-0.69}$) [24], this can lead to higher values for $H_{98}(y, 2)$.

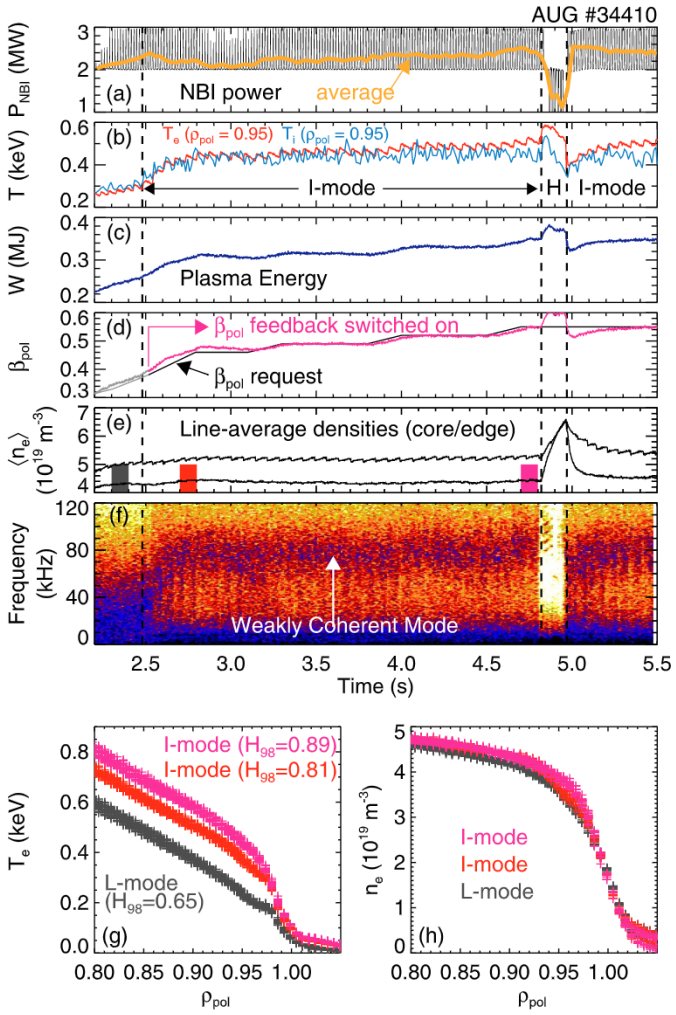

Fig. 1. Stationary I-mode with NBI feedback control on the value of β_{pol}. (a) NBI power, (b) pedestal top electron and ion temperatures, (c) plasma energy, (d) β_{pol} request (black) and measurement (magenta), (e) Line-average densities, (f) density fluctuation spectrogram at $\rho_{pol} = 0.99$, (g) electron temperature profiles, (h) density profiles. The time windows for (f) and (g) are marked in (e).

Another important observation in this discharge is the I-H transition at $t = 4.82$ s. As soon as the plasma goes into H-mode, the density rises strongly, and due to the β_{pol} feedback control, the NBI heating power is reduced and the plasma undergoes an H-I backtransition at $t = 4.97$ s, recovering the I-mode with the same characteristics as before the H-mode appeared. Note the fast loss of density at the H-I transition which underlines the L-mode like particle confinement of the I-mode.Transients in density during the edge pedestal buildup after the L-H transition on AUG have been extensively analyzed through transport analysis [25]. A similar study for I-H and H-I transitions is out of the scope of this paper and left for future work.

Fig. 1(f) depicts the density fluctuation spectrogram measured by reflectometry at $\rho_{pol} = 0.99$ [26]. Clearly, the WCM is dominating the spectrum during the I-mode phase, while in L-mode, it is not visible. Note also the drastic reduction of density fluctuations during the short H-mode phase and the immediate recovery of the WCM after the H-I transition.

3. Detailed investigation of the weakly coherent mode

The weakly coherent mode (WCM) has been observed during I-mode operation on Alcator C-Mod [5] and AUG [7] and has often been identified as a characteristic feature of the I-mode. It has been observed to be coupled to the Geodesic Acoustic Mode [6,7]. The WCM has also been studied with BOUT++ simulations [8], and some agreement with the experiment in terms of frequency and width of the mode has been obtained. Furthermore, the WCM is linked to pronounced density turbulence bursts [9]. These turbulence bursts exist at various structure sizes ($k_\perp$ = 5–12 cm^{-1}, with $k_\perp$ the perpendicular wavenumber of density fluctuations), and after their generation, density and energy is expelled from the confined plasma and deposited in the divertor [10]. These points show that, indeed, the WCM plays a significant role in I-mode, at least on C-Mod and AUG. However, as will be shown in the following, the WCM isnot exclusive to I-mode. In fact, I-modes on DIII-D usually do not exhibit a WCM comparable to that of Alcator C-Mod or AUG [27]. Furthermore, signatures of the WCM surviving an I-L transition have been observed on Alcator C-Mod [6].

Recent studies on AUG show that a mode can be observed in L-mode which seems likely to be the WCM, although it is somewhat more narrow, hence more coherent. This is illustrated in Fig. 2. The NBI input power P_{NBI} (panel (a)) is slightly increased, and at t = 2.74 s, the plasma enters I-mode. The increased energy confinement is visible in the ion and electron pedestal top temperatures (c) and in the plasma stored energy (d). In I-mode, the stored energy increases faster with the heating power ramp than in L-mode. Note that the density (panel (b)) does not change during the L-I transition. At t = 2.96 s, the I-H transition takes place, and the density increases due to the improved particle confinement in H-mode.

Fig. 2(e) and (f) show spectrograms of temperature fluctuations measured by correlation electron cyclotron emission (CECE) [28] and coherent density fluctuations measured by poloidal correlation reflectometry (PCR) [26] in the plasma edge (ρ_{pol} = 0.99).The optical depth for the CECE measurement is 2.8 in L-mode and 3.9 in I-mode. If the measurement were dominated by density fluctuations, the value of $\delta n/n$ would have to be about 30% in L-mode and 70% in I-mode (assuming a wall reflectivity of 0.8). This is not the case, as will be shown later via measurements of a thermal helium beam. The temperature perturbation associated with the WCM in Fig. 2(e) is 2.0% in L-mode and rises slowly to 2.3% in I-mode. These values are consistent with findings from Alcator C-Mod, where values of $\sim$ 1 – 2% have been measured [29]. During the I-mode phase of the discharge, the WCM dominates both the density and temperature spectra, and its frequency increases from $f_{WCM} \approx$ 50 kHz at the beginning of the I-mode to 80 kHz just before the H-mode starts. This is the WCM which is usually related to I-mode [5–7,9]. However, both density and temperature spectra indicate that a mode exists in L-mode long before the I-mode starts. Note that this mode is significantly narrower and hence more coherent than the WCM is in I-mode. However, although the mode has lower frequency in L-mode than the WCM of the late I-mode, it goes smoothly over into the WCM at the L-I transition. This makes it seem likely that it is actually the WCM, which exists already in L-mode, but changes its frequency and width in I-mode. Panel (f) shows the coherence of two poloidally displaced reflectometry channels, which becomes stronger in I-mode. This does not necessarily mean that the WCM itself is stronger in I-mode. A reduction of background turbulence – as observed on both Alcator C-Mod and AUG – can also lead to a more pronounced coherence of the mode. Indeed, the spectrogram of density fluctuations measured with reflectometry (Fig. 2(g)), does not show an increase of the density fluctuation power associated with the WCM in I-mode. It does show, however, a significant increase in low-frequency ($<$ 10 kHz) broadband fluctuations in the I-mode. It should be pointed out that this increase in low frequency fluctuations is not always seen (cf Fig. 1(f)), and thus seems not to be connected directly to the I-mode regime.

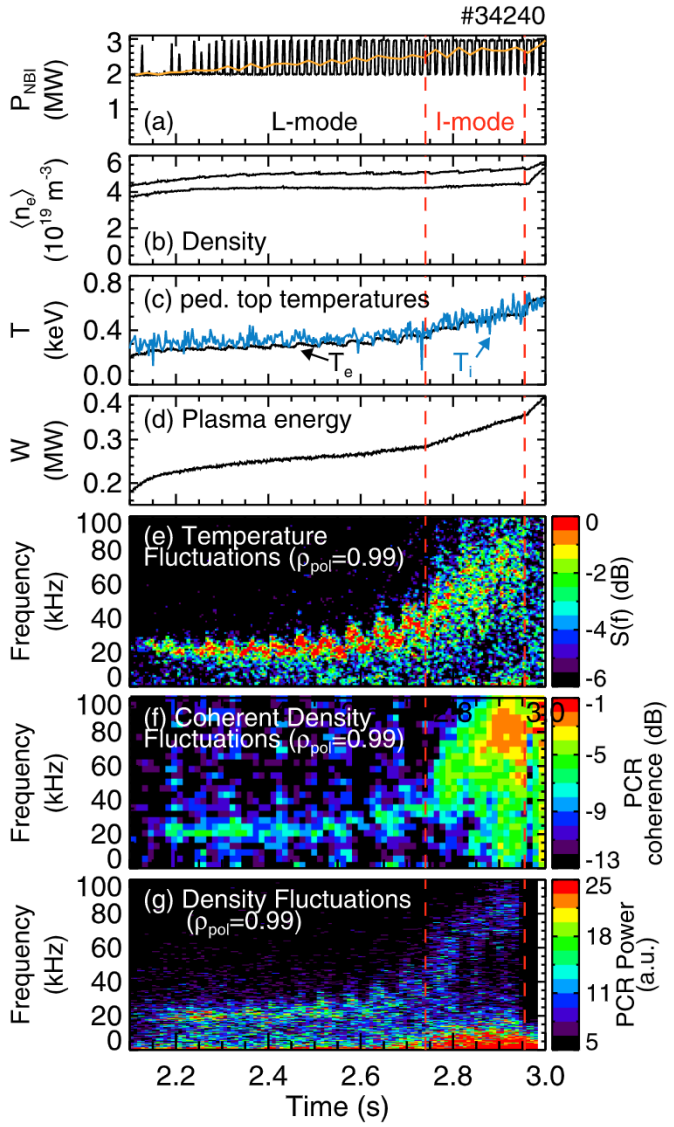

Fig. 2. Time evolution of NBI power (orange: average) (a), line-average core and edge density (b), electron and ion pedestal top temperatures (c), plasma stored energy (d), electron temperature fluctuations(e), density fluctuation coherence (f), density fluctuation spectrogram (g), in a plasma with an L-mode and an I-mode phase on AUG.

A new thermal helium beam diagnostic on AUG [30,31] has been used to study the effect of the WCM on edge density and temperature fluctuations, which are measured with high spatial and temporal resolution in the plasma edge and scrape-off layer (SOL).The diagnostic is based on a line ratio technique. By measuring at least three line intensities, two line ratios can be formed. Combined with a collisional radiative model (CRM), n_e and $T_e$can be calculated and disentangled [32]. Although the values of the two line ratios change with changing n_e and T_e [33], the application of the CRM disentangles the two contributions up to the experimentally given uncertainty of n_e and T_e.

The WCM waveforms in electron density and temperature are shown in Fig. 3(a–e) and (f–j), respectively. For the plot, 153 time windows of 90 μs duration from AUG discharge #34640 at t = 3.68 – 3.75 s have been identified and coherently averaged. The phase locking is achieved by using a density turbulence burst (cf. Refs [9,10].) as reference. Fig. 3(a) shows the density fluctuations caused by the WCM at four radial positions: two inside the last closed flux surface (LCFS), and two outside. Uncertainties are shown as a grey area exemplarily for the innermost position. The relative uncertainties for the

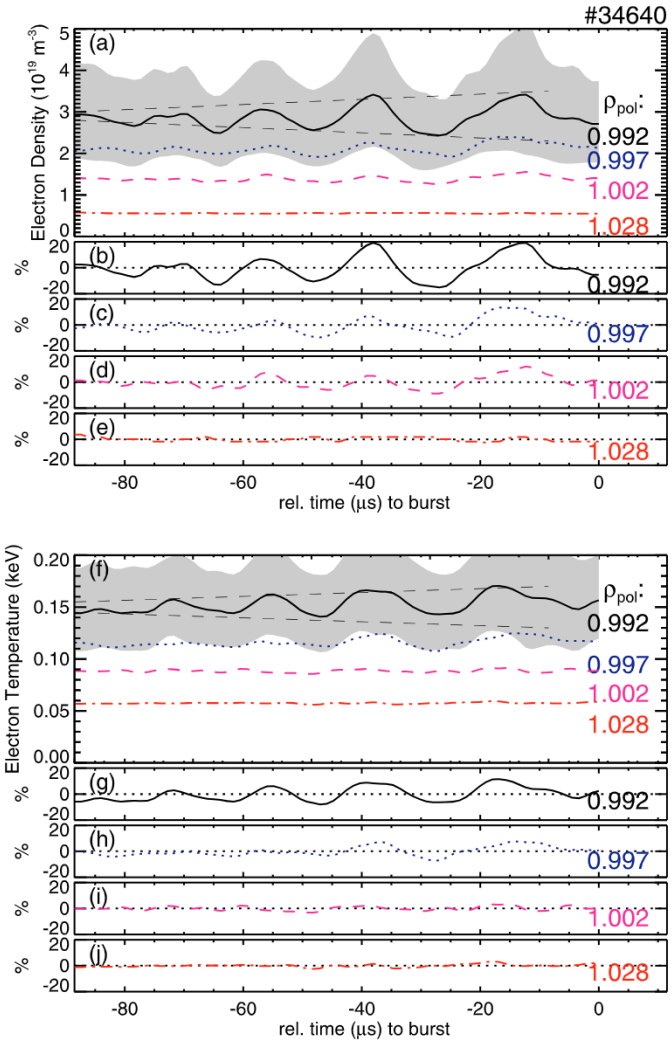

Fig. 3. Averaged edge and near-SOL measurements obtained with a thermal Helium beam of the weakly coherent mode in (a) electron density and (f) electron temperature just before a density burst occurs (at 90 μs). (b–e) and (g–j) show the relative changes. For details refer to the text.

other positions are comparable. They are obtained by using the standard deviation of the 153 time windows. While the WCM is clearly visible at radial positions inside the separatrix (black solid and blue dotted), its impact is reduced once the separatrix is reached and further outside in the SOL (magenta dashed and red dashed-dotted). During the time window, the WCM amplitude increases. To guide the eye, dashed lines are drawn for the innermost measurement position. The growth in WCM amplitude reminds of the growth of the WCM precursor events just before the burst appears [9,10]. Fig. 3(b–e) show the relative fluctuation amplitudes caused by the WCM on the density. The strongest impact is at the innermost position ($\rho_{pol} = 0.992$) and amounts to relative amplitudes of roughly 20%. Equivalent time traces for the electron temperature at the same radial positions are shown in Fig. 3(f–j). Basically, the trend is similar in that the WCM is visible inside the confined plasma but not outside. However, the temperature fluctuation amplitudes connected to the WCM amount only to 10%. This means that the relative fluctuation amplitudes of the WCM are twice as high for the density compared to the temperature. No significant phase difference can be observed between the density and temperature waveforms of the WCM.Note the temperature perturbation obtained with this method is larger than that of the CECE measurement, which is probably due to a combination of two reasons: first, the thermal helium beam analysis is conditionally averaged to obtain a representative waveform of the WCM just before a turbulence burst appears. Since the WCM is related to these bursts, it is reasonable to assume that predominantly, higher WCM amplitudes will be extracted through such an analysis. Second, the helium beam channels are radially relatively narrow (~ 5 mm), and it could be that the radial CECE extension (~ 10 mm) causes some smearing, and hence lower values for $\delta T/T$. These results are highly consistent with those published from Alcator C-Mod [29] in the following aspects: (i) the WCM is observed only in the confinement region, (ii) the temperature perturbation is smaller than the density perturbation, (iii) the density perturbation is of the order of 10 – 20%

Summarizing the above, it is highly probable that the WCM is not exclusive to I-mode, at least in AUG. However, since in I-mode the background turbulence is strongly suppressed, it dominates the fluctuating quantities. It seems likely that due to this suppression of background turbulence, the WCM couples to the density turbulence bursts [9,10]. Furthermore, the WCM is clearly seen in both electron density and temperature, and it exists in the edge pressure gradient region inside the LCFS. The WCM impact on density is about twice as strong as it is on the temperature. These observations further strengthen the idea that the WCM is responsible for the edge particle transport in I-mode [5].

4. Divertor heat loads and power fall-off lengths

For any future device and operational regime, the divertor heat load is of particular importance. In any device in equilibrium, the heat fluxes from the core plasma due to external heating and internal alpha heating will partly be radiated, but a large fraction will cross the separatrix and flow along the magnetic field lines into the divertor. Since the parallel transport is fast compared to the perpendicular transport, a large fraction of this power will be deposited in a narrow region in the divertor, quantified by the so-called power fall-off length λ_q [34,35]. In the present paper, λ_q refers to the power fall-off length mapped to the outer midplane. Large values for λ_q are beneficial, since the power crossing the separatrix is spread onto a larger area in the divertor. Usually, in L-mode and H-mode, due to Spitzer-Härm conductivity, a scaling of $\lambda_q \approx 2/7\lambda_{T_e}$ is obtained [16,17,36]. Since λ_{T_e} is roughly a factor of two smaller in H-mode than in L-mode [17], this makes the problem even larger in H-mode. Investigations done by Terry et al. on Alcator C-Mod have shown that λ_q in I-mode is significantly larger than in H-mode [18], which could be due to less volume-averaged pressure in I-mode [19]. This section investigates both stationary (Section 4.1) and transient divertor heat loads (Section 4.2) in I-mode. The latter are caused by the WCM in connection with the intermittent turbulence bursts from the confinement region.

4.1. Stationary divertor heat loads

Fig. 4(a–d) shows heat flux profiles from the outer divertor for L-mode (a), two different I-mode time points (b,c), and inter-ELM H-mode (d). To obtain these data, the IR-thermography diagnostic has been used, which measures the temperature of a divertor tile. The temporal evolution of the tile temperature allows one to infer the heat flux density by solving the heat diffusion equation inside the tile [37]. A fit reflecting a Gaussian convolved with an exponential is used to characterize the power fall-off length λ_q. For details, see Refs [35,36,38].

The H-mode profile (d) is narrower and shows a more pronounced decay than the L-mode profile (a). Also, the peak heat flux value is reduced in H-mode w.r.t. L-mode. This is because some of the heat is transported out of the plasma via type-I ELMs, and in this discharge the radiated power in the H-mode phase is a factor 2 above the radiated power in the L-mode phase. The width of the I-mode heat flux profiles (b,c) is in between those of L-mode and H-mode. Fig. 4(c) shows an interesting feature observed in late I-modes: some of the heat flux profiles exhibit higher values than those in early I-mode. This is related

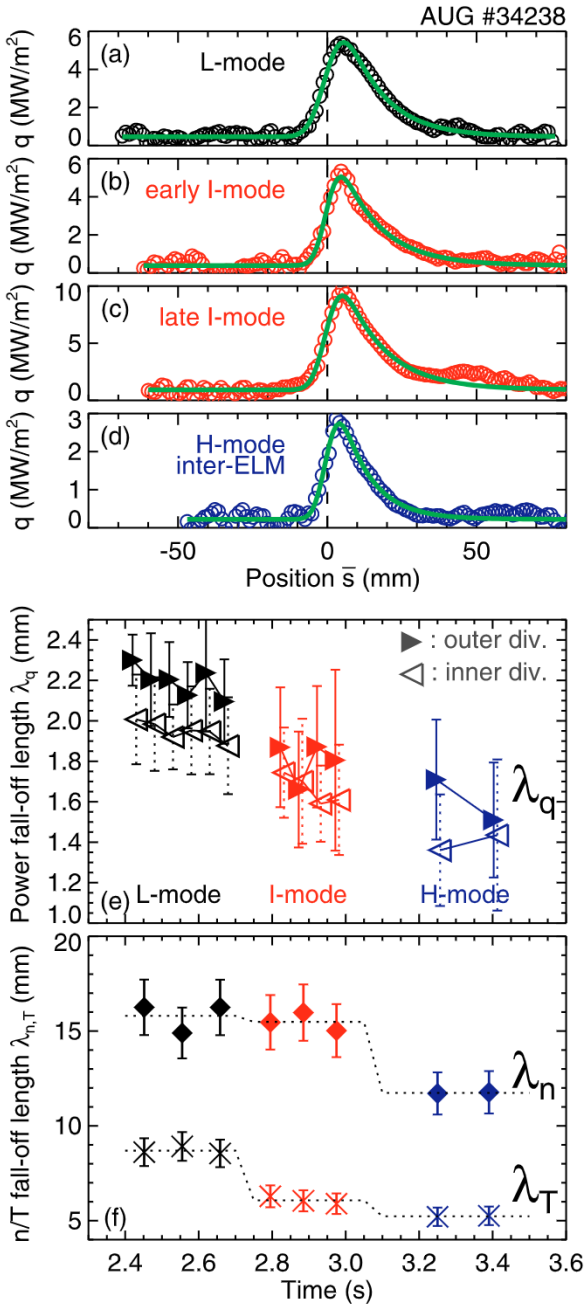

Fig. 4. Example outer divertor heat flux profiles for (a) L-mode, (b) early I-mode, (c) late I-mode, (d) H-mode. The late I-mode profile shows a second bump at 115 mm, which is due to the bursty character of late I-mode phases. See Section. 4.2 for details. (e) Power fall-off length λ_q (mapped to the outer midplane) during a L-, I- and H-mode transition on AUG and (f) corresponding SOL density and temperature fall-off lengths with dotted lines to guide the eye. For details, refer to the text.

to the intermittent and bursty transport increasing with I-mode confinement quality [9]. More details on the intermittent bursty transport are reported in Section 4.2 and Refs [9,10,39].

Fig. 4(e) shows the temporal evolution of λ_q for a plasma going from L-mode through I-mode into H-mode. The measurements have been obtained on both the outer (▶) and the inner (◁) divertor. One might expect that the value of λ_q obtained from the outer and inner divertor measurements should be equivalent as both are mapped to the outer midplane. However, Fig. 4 shows that there is a slight discrepancy, where λ_q obtained from the inner divertor measurements is below the values obtained from the outer divertor measurements. This could be due to the vertical magnetic drifts of ions and the plasma triangularity [36,40–42]. Nevertheless, the relative changes of λ_q are independent of whether the values are obtained from inner or outer divertor measurements. From L-mode (black) to I-mode (red), there is a slight reduction of λ_q from roughly 2.1 mm to 1.7 mm. In H-mode, $\lambda_q \approx 1.5$ mm. These results confirm measurements from Alcator C-Mod [18,19]. However, it should be noted that if a future device is built with a standard divertor, then attached I-modes will deposit too much energy on the divertor. Therefore, it is necessary to study whether it is possible to obtain detachment in I-mode. Corresponding experiments are planned for the near future on AUG.

The density and electron temperature fall-off lengths measured with the Thomson scattering system [43] are depicted in Fig. 4(f). While λ_T is reduced from L-mode to I-mode, λ_n stays at the same value. This is reminiscent of the decoupling of energy and transport channels in I-mode. Only when the plasma goes into H-mode is λ_n reduced, while λ_T barely changes. The temperature fall-off length in I-mode is $\lambda_T \approx 6$ mm, the power fall-off length $\lambda_q \approx 1.7$ mm, which indicates that the I-mode SOL is dominated by Spitzer-Härm conductivity, which relates both quantities through $\lambda_q = 2/7\lambda_T$.More information on $\lambda_n$and λ_T in different confinement regimes on AUG can be found in Ref. [15].

4.2. Transient divertor heat loads

As mentioned before, apart from stationary divertor heat loads, the I-mode also exhibits an increased degree of intermittency, which is also reflected by observations in the divertor.

Fig. 5shows a time window including L-mode, I-mode and H-mode, which displays a large degree of intermittent fluctuations in the I-mode phase. Panel (a) shows the pedestal top electron temperature, which is roughly 330 eV in L-mode and starts to increase at $t = 4.1$ s, when I-mode is entered. About one confinement time later, at $t = 4.2$ s, it has reached 440 eV, which is an increase of 33%. Once the higher pedestal top temperature is established, small dips appear at irregular time intervals in T_e. These dips correspond to the turbulence bursts already

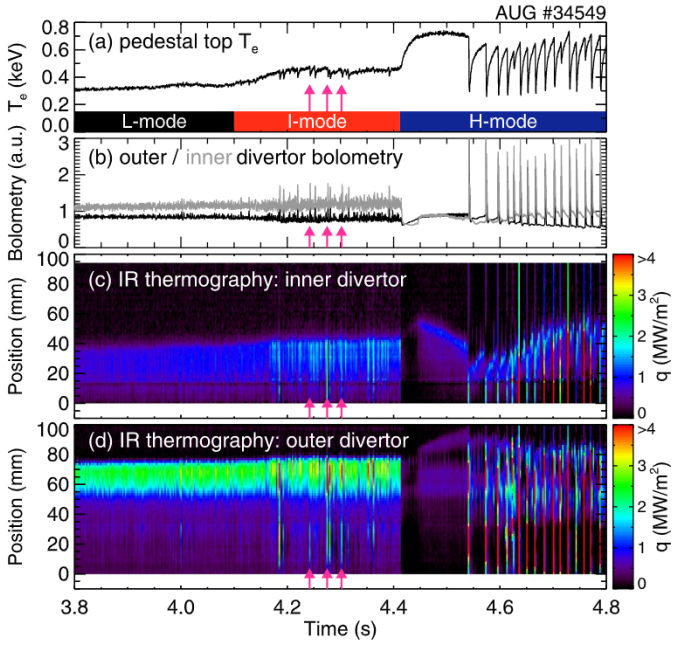

Fig. 5. Time traces of (a) pedestal top electron temperature, (b) AXUV bolometry, heat flux in inner (c) and outer (d) divertor. In I-mode, bursty behavior and transient divertor heat loads are observed, related to dips in the pedestal top electron temperature and the bolometry bursts (marked by arrows). The type-I ELMs at the end of the time window show a rather different signature than the I-mode bursts. For details, refer to the text.

reported in [9,10,39]. As pointed out previously, the I-mode edge is a factor of three away from the peeling-ballooning instability boundary [10,11], which means that these events are not type-I ELMs. The plasma energy loss associated with the bursts is at maximum $\Delta W/W = 1.5\%$. At $t = 4.415$ s, the plasma enters H-mode, which is seen in a further increase of the pedestal top T_e. The type-I ELMs in the later H-mode phase are very pronounced and cause an energy loss of roughly $\Delta W/W = 7.3\%$. By comparison with the I-mode dips it becomes clear that the I-mode events are quite different from type-I ELMs.

For comparison, panel (b) shows measurements from an absolute extended ultraviolet (AXUV) diode based bolometer diagnostic [44]. Depicted are two lines of sight which impact the inner and outer divertor. In I-mode, the intermittent behavior is confirmed also from bolometry measurements. Note that the radiation is significantly reduced at the sharp drop of the signal at the I-H transition, and that the signal caused by the ELMs is significantly different from the I-mode burst induced bolometry response.

The divertor heat fluxes are plotted in panels (c) and (d) for the inner and outer divertor, respectively. The y-axis is a spatial coordinate along the divertor target. In L-mode, the heat fluxes are comparably smooth and few fluctuations are visible. This does not change substantially when I-mode is entered ($t = 4.1$ s). However, as soon as the I-mode temperature pedestal is established at $t \approx 4.2$ s, strong divertor heat loads related to the small T_e dips from panel (a) are measured on both outer and inner divertor. This intermittent behavior only ceases when the ELM-free phase of the H-mode starts. Later, the ELMs are clearly visible in the divertor heat load signals.Unfortunately, due to the short duration of the turbulence bursts (about 50 μs) and the limited time resolution of the IR diagnostic in this discharge (2.3 ms), it is not possible at the moment to give an estimate of burst-related heat fluxes. It is planned to conduct dedicated experiments in the near future, in which long time series with many bursts will be acquired. This will enable the estimation of heat fluxes through statistical methods.

In summary, divertor heat loads in I-mode are seen of both stationary type, where λ_q is between those of L- and H-mode, and transient type, where intermittent events are observed, which impact the divertor. Future studies are necessary in order to quantify exactly the heat fluxes associated with the intermittent bursts, which are generated in the confinement region and linked to the WCM.

5. Summary

Recent studies of the I-mode confinement regime from the AUG tokamak have been reported. In particular, it has been shown that with the application of NBI feedback control, stationary I-modes can robustly be maintained. This is not only of particular importance for studies which require long time series (e.g. IR thermography, studies of SOL fall-off lengths), but also with regard to future devices, where I-mode could be envisaged as an operational regime. Furthermore, H-I transitions have been observed which recover all I-mode properties, namely good energy confinement, L-mode like particle transport, and the weakly coherent mode (WCM). These points show that the I-mode is a robust confinement regime, which can be obtained irrespective of the discharge history.

Furthermore, new investigations of the WCM show that it might not be exclusive to I-mode, but can exist in L-mode too. However, the WCM could be important for the I-mode regime to keep the density transport on an L-mode level, because the background density turbulence is largely reduced in I-mode. It has been speculated that the WCM is at least partly responsible for the density transport [5,8], in particular with the connection to the density bursts observed on AUG [9,10]. Moreover, it could be determined that the WCM impact is strongest inside the separatrix and that it is barely visible in the SOL. The relative fluctuation amplitudes of the WCM are twice as high for the density compared to the temperature.

Divertor heat fluxes have been analyzed for the first time for AUG I-modes. It has been found that the power fall-off length λ_q in I-mode is smaller than in L-mode, but also larger than in H-mode, and it scales with the scrape-off layer temperature fall-off length λ_T. Furthermore, it has been shown that the divertor experiences transient heat loads in I-mode. These transient heat loads are caused by so-called turbulence bursts, which are generated in the confined edge plasma and linked to the WCM, whose dominance in the density fluctuation spectrum is closely related to I-mode. These bursts are not type-I ELMs, which typically cause significantly larger divertor heat loads.

Acknowledgments

This work was partly performed within the framework of the EUROfusion Consortium and has received funding from the Euratom research and training programme 2014-2018 under grant agreement No 633053. Furthermore, funding from the EUROfusion Enabling Research work-package AWP15-ENR-09/IPP-02 is acknowledged. The views and opinions expressed herein do not necessarily reflect those of the European Commission. This work is supported by the US DOE under grants DE-SC0006419 and DE-SC0017381.

References

[1] F. Ryter, W. Suttrop, B. Brüsehaber, M. Kaufmann, V. Mertens, H. Murmann, A.G. Peeters, J. Stober, J. Schweinzer, H. Zohm, the ASDEX Upgrade Team, Plasma Phys. Control. Fusion 40 (1998) 725.
[2] D.G. Whyte, A.E. Hubbard, J.W. Hughes, B. Lipschultz, J.E. Rice, E.S. Marmar, M. Greenwald, I. Cziegler, A. Dominguez, T. Golfinopoulos, N. Howard, L. Lin, R.M. McDermott, M. Porkolab, M.L. Reinke, J. Terry, N. Tsujii, S. Wolfe, S. Wukitch, Y. Lin, the Alcator C-Mod Team, Nucl. Fusion 50 (2010) 105005.
[3] J. Rice, M. Reinke, C. Gao, N. Howard, M. Chilenski, L. Delgado-Aparicio, R. Granetz, M. Greenwald, A. Hubbard, J. Hughes, J. Irby, Y. Lin, E. Marmar, R. Mumgaard, S. Scott, J. Terry, J. Walk, A. White, D. Whyte, S. Wolfe, S. Wukitch, Nucl. Fusion 55 (2015) 033014.
[4] S. Espinosa, P.J. Catto, Plasma Phys. Control. Fusion 60 (2018) 094001.
[5] A.E. Hubbard, D.G. Whyte, R.M. Churchill, I. Cziegler, A. Dominguez, T. Golfinopoulos, J.W. Hughes, J.E. Rice, I. Bespamyatnov, M.J. Greenwald, N. Howard, B. Lipschultz, E.S. Marmar, M.L. Reinke, W.L. Rowan, J.L. Terry, the Alcator C-Mod Group, Phys. Plasmas 18 (2011) 056115.
[6] I. Cziegler, P.H. Diamond, N. Fedorczak, P. Manz, G.R. Tynan, M. Xu, R.M. Churchill, A.E. Hubbard, B. Lipschultz, J.M. Sierchio, J.L. Terry, C. Theiler, Phys. Plasmas 20 (2013) 055904.
[7] P. Manz, P. Lauber, V. Nikolaeva, T. Happel, F. Ryter, G. Birkenmeier, A. Bogomolov, G. Conway, M. Manso, M. Maraschek, D. Prisiazhniuk, E. Viezzer, the ASDEX Upgrade Team, Nucl. Fusion 55 (2015) 083004.
[8] Z.X. Liu, X.Q. Xu, X. Gao, A.E. Hubbard, J.W. Hughes, J.R. Walk, C. Theiler, T.Y. Xia, S.G. Baek, T. Golfinopoulos, D. Whyte, T. Zhang, J.G. Li, Phys. Plasmas 23 (2016) 120703.
[9] T. Happel, P. Manz, F. Ryter, P. Hennequin, A. Hetzenecker, G. Conway, L. Guimarais, C. Honoré, U. Stroth, E. Viezzer, the ASDEX Upgrade Team, Nucl. Fusion 56 (2016) 064004.
[10] T. Happel, P. Manz, F. Ryter, M. Bernert, M. Dunne, P. Hennequin, A. Hetzenecker, U. Stroth, G.D. Conway, L. Guimarais, C. Honoré, E. Viezzer, The ASDEX Upgrade Team, Plasma Phys. Control. Fusion 59 (2017) 014004.
[11] J.R. Walk, J.W. Hughes, A.E. Hubbard, J.L. Terry, D.G. Whyte, A.E. White, S.G. Baek, M.L. Reinke, C. Theiler, R.M. Churchill, J.E. Rice, P.B. Snyder, T. Osborne, A. Dominguez, I. Cziegler, Phys. Plasmas 21 (2014) 056103.
[12] A. Hubbard, S.G. Baek, D. Brunner, A. Creely, I. Cziegler, E. Edlund, J. Hughes, B. LaBombard, Y. Lin, Z. Liu, E. Marmar, M. Reinke, J. Rice, B. Sorbom, C. Sung, J. Terry, C. Theiler, E. Tolman, J. Walk, A. White, D. Whyte, S. Wolfe, S. Wukitch, X. Xu, the Alcator C-Mod team, Nucl. Fusion 57 (2017) 126039.
[13] B. Sorbom, J. Ball, T. Palmer, F. Mangiarotti, J. Sierchio, P. Bonoli, C. Kasten, D. Sutherland, H. Barnard, C. Haakonsen, J. Goh, C. Sung, D. whyte, Fusion Eng. Des. 100 (2015) 378.
[14] B. LaBombard, E. Marmar, J. Irby, J. Terry, R. Vieira, G. Wallace, D. Whyte, S. Wolfe, S. Wukitch, S. Baek, W. Beck, P. Bonoli, D. Brunner, J. Doody, R. Ellis, D. Ernst, C. Fiore, J. Freidberg, T. Golfinopoulos, R. Granetz, M. Greenwald, Z. Hartwig, A. Hubbard, J. Hughes, I. Hutchinson, C. Kessel, M. Kotschenreuther, R. Leccacorvi, Y. Lin, B. Lipschultz, S. Mahajan, J. Minervini, R. Mumgaard, R. Nygren, R. Parker, F. Poli, M. Porkolab, M. Reinke, J. Rice, T. Rognlien, W. Rowan, S. Shiraiwa, D. Terry, C. Theiler, P. Titus, M. Umansky, P. Valanju, J. Walk, A. White, J. Wilson, G. Wright, S. Zweben, Nucl. Fusion 55 (2015) 053020.
[15] H.J. Sun, E. Wolfrum, T. Eich, B. Kurzan, A. Kallenbach, T. Happel, U. Stroth, the ASDEX Upgrade Team, Plasma Phys. Control. Fusion 61 (2019) 014005.
[16] H.J. Sun, E. Wolfrum, T. Eich, B. Kurzan, S. Potzel, U. Stroth, the ASDEX Upgrade Team, Plasma Phys. Control. Fusion 57 (2015) 125011.
[17] H.J. Sun, E. Wolfrum, B. Kurzan, T. Eich, K. Lackner, A. Scarabosio, I.P. Pérez, O. Kardaun, M. Faitsch, S. Potzel, U. Stroth, the ASDEX Upgrade Team, Plasma Phys. Control. Fusion 59 (2017) 105010.

[18] J. Terry, B. LaBombard, D. Brunner, J. Hughes, M. Reinke, D. Whyte, J. Nucl. Mat. 438 (2013) S212. Proceedings of the 20th International Conference on Plasma-Surface Interactions in Controlled Fusion Devices
[19] D. Brunner, B. LaBombard, A. Kuang, J. Terry, Nucl. Fusion 58 (2018) 094002.
[20] F. Ryter, R. Fischer, J. Fuchs, T. Happel, R. McDermott, E. Viezzer, E. Wolfrum, L.B. Orte, M. Bernert, A. Burckhart, S.d. Graca, B. Kurzan, P. McCarthy, T. Pütterich, W. Suttrop, M. Willensdorfer, the ASDEX Upgrade Team, Nucl. Fusion 57 (2017) 016004.
[21] A. Hubbard, T. Osborne, F. Ryter, M. Austin, L.B. Orte, R. Churchill, I. Cziegler, M. Fenstermacher, R. Fischer, S. Gerhardt, R. Groebner, P. Gohil, T. Happel, J. Hughes, A. Loarte, R. Maingi, P. Manz, A. Marinoni, E. Marmar, R. McDermott, G. McKee, T. Rhodes, J. Rice, L. Schmitz, C. Theiler, E. Viezzer, J. Walk, A. White, D. Whyte, S. Wolfe, E. Wolfrum, Z. Yan, the Alcator C-Mod, ASDEX Upgrade and DIII-D Teams, Nucl. Fusion 56 (2016) 086003.
[22] R. Fischer, C.J. Fuchs, B. Kurzan, W. Suttrop, E. Wolfrum, A. U. Team, Fusion Sci. Technol. 58 (2010) 675.
[23] ITER Physics Basis Editors, ITER Physics Expert Group Chairs and Co-Chairs, ITER Joint Central Team, Physics Integration Unit, Nucl. Fusion 39 (1999) 2137.
[24] ITER Physics Expert Group on Confinement and Transport, ITER Physics Expert Group on Confinement Modelling and Database, ITER Physics Basis Editors, Nucl. Fusion 39 (1999) 2175.
[25] M. Willensdorfer, E. Fable, E. Wolfrum, L. Aho-Mantila, F. Aumayr, R. Fischer, F. Reimold, F. Ryter, the ASDEX Upgrade Team, Nucl. Fusion 53 (2013) 093020.
[26] D. Prisiazhniuk, A. Krämer-Flecken, G.D. Conway, T. Happel, A. Lebschy, P. Manz, V. Nikolaeva, U. Stroth, the ASDEX Upgrade Team, Plasma Phys. Control. Fusion 59 (2017) 025013.
[27] A. Marinoni, J. Rost, M. Porkolab, A. Hubbard, T. Osborne, A. White, D. Whyte, T. Rhodes, E. Davis, D. Ernst, K. Burrell, Nucl. Fusion 55 (2015) 093019.
[28] S.J. Freethy, G.D. Conway, I. Classen, A.J. Creely, T. Happel, A. Köhn, B. Vanovac, A.E. White, Rev. Sci. Instrum. 87 (2016) 11E102.
[29] A. White, P. Phillips, D. Whyte, A. Hubbard, C. Sung, J. Hughes, A. Dominguez, J. Terry, I. Cziegler, Nucl. Fusion 51 (2011) 113005.
[30] M. Griener, J.M.M. Burgos, M. Cavedon, G. Birkenmeier, R. Dux, B. Kurzan, O. Schmitz, B. Sieglin, U. Stroth, E. Viezzer, E. Wolfrum, the ASDEX Upgrade Team, Plasma Phys. Control. Fusion 60 (2018) 025008.
[31] M. Griener, E. Wolfrum, M. Cavedon, R. Dux, V. Rohde, M. Sochor, J.M.M.n. Burgos, O. Schmitz, U. Stroth, Rev. Sci. Instrum. 89 (2018) 10D102.
[32] U. Kruezi, H. Stoschus, B. Schweer, G. Sergienko, U. Samm, Rev. Sci. Instrum. 83 (2012) 065107.
[33] M. Griener, (2018) Ph.d. thesis.
[34] A. Loarte, S. Bosch, A. Chankin, S. Clement, A. Herrmann, D. Hill, K. Itami, J. Lingertat, B. Lipschultz, K. McCormick, R. Monk, G. Porter, M. Shimada, M. Sugihara, J. Nucl. Mat. 266–269 (1999) 587.
[35] T. Eich, B. Sieglin, A. Scarabosio, W. Fundamenski, R.J. Goldston, A. Herrmann, Phys. Rev. Lett. 107 (2011) 215001.
[36] M. Faitsch, B. Sieglin, T. Eich, H.J. Sun, A. Herrmann, the ASDEX Upgrade Team, Plasma Phys. Control. Fusion 57 (2015) 075005.
[37] B. Sieglin, M. Faitsch, A. Herrmann, B. Brucker, T. Eich, L. Kammerloher, S. Martinov, Rev. Sci. Instrum. 86 (2015) 113502.
[38] T. Eich, A. Leonard, R. Pitts, W. Fundamenski, R. Goldston, T. Gray, A. Herrmann, A. Kirk, A. Kallenbach, O. Kardaun, A. Kukushkin, B. LaBombard, R. Maingi, M. Makowski, A. Scarabosio, B. Sieglin, J. Terry, A. Thornton, A.U. Team, J.E. Contributors, Nucl. Fusion 53 (2013) 093031.
[39] P. Manz, T. Happel, F. Ryter, M. Bernert, G. Birkenmeier, G. Conway, M. Dunne, L. Guimarais, P. Hennequin, A. Hetzenecker, C. Honoré, P. Lauber, M. Maraschek, V. Nikolaeva, D. Prisiazhniuk, U. Stroth, E. Viezzer, The ASDEX Upgrade Team, Nucl. Fusion 57 (2017) 086022.
[40] R. Goldston, Nucl. Fusion 52 (2012) 013009.
[41] B. Sieglin, T. Eich, M. Faitsch, A. Herrmann, A. Scarabosio, the ASDEX Upgrade Team, Plasma Phys. Control. Fusion 58 (2016) 055015.
[42] M. Faitsch, R. Maurizio, A. Gallo, S. Coda, T. Eich, B. Labit, A. Merle, H. Reimerdes, B. Sieglin, C. Theiler, the Eurofusion MST1 Team, the TCV Team, Plasma Phys. Control. Fusion 60 (2018) 045010.
[43] B. Kurzan, H.D. Murmann, Rev. Sci. Instrum. 82 (2011) 103501.
[44] M. Bernert, T. Eich, A. Burckhart, J.C. Fuchs, L. Giannone, A. Kallenbach, R.M. McDermott, B. Sieglin, the ASDEX Upgrade Team, Rev. Sci. Instrum. 85 (2014) 033503.